

# "Needle" Vavilov-Cerenkov radiation in a Rochelle salt crystal

V. P. Zrelov, P. Pavlovich, and P. Sulek

Joint Institute for Nuclear Research

(Submitted July 12, 1972)

Zh. Eksp. Teor. Fiz. **64**, 245-253 (January 1973)

The main properties of Vavilov-Cerenkov radiation in a biaxial Rochelle salt crystal (RSC) with a polydomain structure were investigated by the photographic technique and by using 660 MeV protons from a synchrocyclotron. All major radiation properties predicted by the Muzikar theory for biaxial crystals are confirmed experimentally. It is shown that the azimuthal distribution of the radiation produced by protons moving along the small bisector of the RSC polarized in the optical axes plane is characteristically needle-shaped. The effect of such factors, as electric fields or temperature, on properties of the Vavilov-Cerenkov radiation in RSC is studied. The azimuthal distribution of the radiation emitted by protons with  $\beta = 0.81$  moving along the small RSC bisector is slightly changed; the distribution is modified by an electric field or temperature. Some possible causes of these features are discussed.

## 1. INTRODUCTION

The small number of experimental studies of the properties of Cerenkov radiation in anisotropic media<sup>[1-3]</sup> pertained only to crystals whose optical properties could be characterized by such macroscopic parameters as the refractive index. However, in crystals with structures having dimensions  $a \gtrsim \lambda$  ( $\lambda$  is the wavelength of the Cerenkov radiation in the optical band), one can attempt to observe the influence of these structures on the directivity properties or the polarization properties of the radiation. We chose for this purpose polydomain Rochelle-salt crystals  $\text{KNaC}_4\text{H}_4\text{O}_6 \cdot 4\text{H}_2\text{O}$ . The domain structure of this crystal is preserved in the temperature range from the upper Curie-Weiss point  $t = +24^\circ\text{C}$  to the lower one  $t = -18^\circ\text{C}$ .

Domains in Rochelle salt crystals (RSC) constitute singular regions of spontaneous polarization  $\mathbf{P}$ , directed parallel or antiparallel to the small bisector, the  $X_3$  axis, shown, for example, in Fig. 1 (the  $X_3$  axis is perpendicular to the plane of the figure). The domain width fluctuates between 0.005 and 0.02 mm, and the width of the domain wall is approximately 2 atomic lattice periods. At  $t = 20^\circ\text{C}$ , the domain walls are  $\sim 43 \text{ \AA}$  thick<sup>[4,5]</sup>.

If the particle moves along the  $X_3$  axis of the RSC with a velocity exceeding the threshold for the appearance of the Cerenkov radiation, then it should excite coherently dipoles oriented parallel or antiparallel to the particle velocity. This can lead, in principle, to the appearance of sharply directional dipole, quadrupole, or even multipole Cerenkov radiation (both electric and magnetic), which can be determined from the characteristic polarization of the radiation and the angular distribution.

In the case of experimental observation of a connection of definite type between elementary radiators that are present in the medium and the properties of the Cerenkov radiation, one could say that the particle is only the stimulus that ensures coherence of the radiation (with the exception of quantum effects), and that the properties of the radiation are determined entirely by the medium.

In the theory of Cerenkov radiation in an isotropic medium, it was pointed out in its time by Frank<sup>[4]</sup> that

the current due to the moving particle can be equivalently replaced by a system of immobile dipoles. The problem of determining the nature of the elementary exciters from the polarization of the luminescence was thoroughly analyzed and investigated by Vavilov<sup>[5]</sup> and his school of physicists. A similar situation should take place in principle also for Cerenkov radiation excited in crystals with ordered electric or magnetic structures having dimensions  $a$  of the order of the wavelength of the emitted radiation.

We describe below experiments aimed at verifying the directivity polarization and azimuthal distribution of Cerenkov radiation in two RSC with different domain

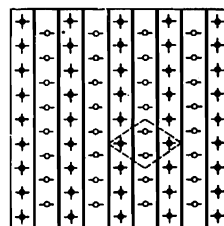


FIG. 1. Plate of  $X_3$ -cut Rochelle salt (viewed along the negative  $X_3$  axis). Double lines—domain walls, diamond—quadrupole.

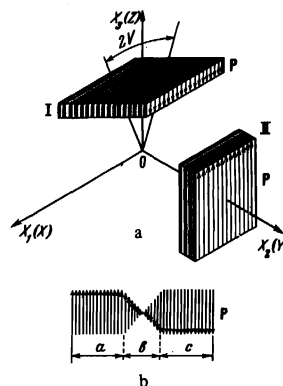


FIG. 2. Rochelle-salt crystal plate with polydomain structure: a—plate I ( $X_3$  cut, perpendicular to the minor bisector) and plate II ( $X_2$  cut); b—direction of the polarization vector  $\mathbf{P}$  in neighboring domains and in the domain wall (angle  $2V = 2\beta$  is the angle between the binormals of the actual crystal).

TABLE I

$\lambda, \text{Å}$	$n_1$	$n_2$	$n_3$	$\lambda, \text{Å}$	$n_1$	$n_2$	$n_3$
4554.2	1.49906	1.50062	1.50504	5853.9	1.49001	1.49183	1.49540
4934.2	1.49565	1.49734	1.50154	6141.9	1.48878	1.49056	1.49430
5535.7	1.49170	1.49348	1.49721	6497	1.48743	1.48920	1.49280

orientations. One Rochelle-salt plate was  $X_3$ -cut, and the second (II) was  $X_2$ -cut with the domains arranged as shown in Fig. 2a. The change in the direction of the polarization vector  $\mathbf{P}$  on going from domain a to the neighboring domain c via the domain wall b is illustrated in Fig. 2b.

The principal refractive indices of the biaxial RSC have (at  $t = 21.3^\circ\text{C}$ ), according to [6], the values listed in Table I.

The angle  $\beta$  between the binormals, calculated from the formula

$$\text{tg } \beta = \sqrt{\frac{\epsilon_3(\epsilon_2 - \epsilon_1)}{\epsilon_1(\epsilon_3 - \epsilon_2)}}$$

at  $\lambda = 6497 \text{ Å}$  ( $2\beta = 70^\circ 13'$ ) agrees with the measurements [7] ( $2\beta = 2V$ ).

## 2. EXPERIMENTAL CONDITIONS

The experimental setup was the same as in the investigation of the properties of the Cerenkov radiation in other crystals [1,2] (see also Fig. 8 below). The RSC were prepared in the form of plane-parallel plates 5 mm thick. Their density, according to [6], was  $\rho_{\text{RSC}} = 1.766 \text{ g/cm}^3$ . At an average RSC atomic number  $Z = 9.14$ , the ionization loss of 660 MeV protons in the crystal is  $\Delta E/\Delta X = 2.12 \text{ MeV-cm}^2/\text{g}$  [8], and the radiation length is  $X_0 = 33 \text{ g/cm}^2$ . The proton energy at the center of the crystal plate was 662 MeV, corresponding to a velocity  $\beta = 0.810065$ , with  $\beta_1 = 0.8094$  in the lens ( $n_D = 1.512 \pm 0.001$  at  $\lambda = 5893 \text{ Å}$ ). The radiation was recorded with negative color film Orwo-color 16 DIN. The total proton flux necessary to obtain a normal negative image was  $\sim 10^{11}$ .

## 3. EXPERIMENTAL RESULTS

**Experiment 1.** Protons with velocity  $\beta = 0.81$  passed through an  $X_3$ -cut RSC plate, i.e., along the minor bisector. The result in this case was the photograph shown

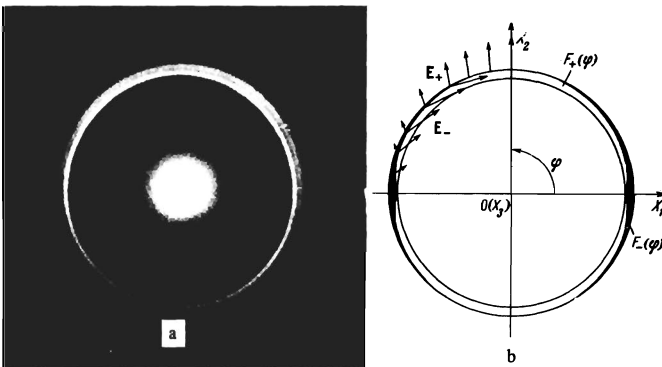


FIG. 3. Experimental and theoretical distributions of Cerenkov radiation  $F_+(\varphi)$  and  $F_-(\varphi)$ , produced when protons with  $\beta = 0.81$  move along the minor bisector ( $X_3$  axis) of a biaxial RSC. a—Experimental distribution obtained with an experimental setup analogous to that of Fig. 8 (outer ring—reference from a lens, inner—from RSC, central spot—imprint of the proton beam). b—Calculated distributions  $F_+(\varphi)$  and  $F_-(\varphi)$  with indication of the polarizations of the waves  $E_+$  and  $E_-$ .

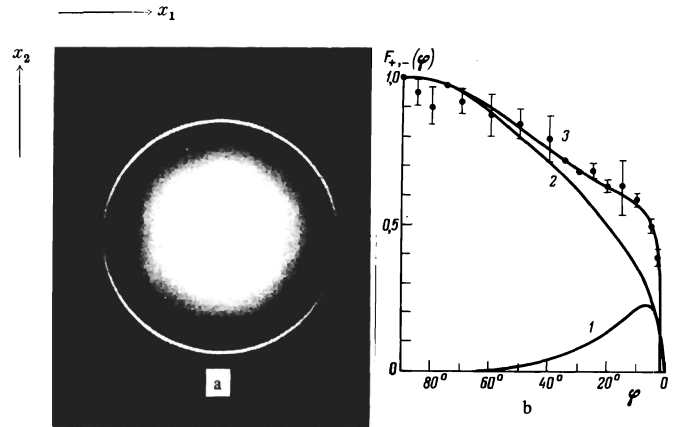


FIG. 4. Plots of the intensities of the waves  $F_+(\varphi)$  and  $F_-(\varphi)$  (produced by passage of protons with  $\beta = 0.81$  along the  $X_3$  axis of the RSC), transmitted through a polaroid oriented along the  $X_2$  axis. a—Photograph of the radiation produced in experiment 1 (inner ring with two "gaps"—radiation from RSC, outer "arcs"—radiation from lens). b—Calculated plots: 1— $F_-(\varphi) \cos^2 \alpha$ , 2— $F_+(\varphi) \cos^2 \alpha$ , and 3— $(F_+(\varphi) + F_-(\varphi)) \cos^2 \alpha$ —smooth curves and experimental plot  $F_e(\varphi)$ .

in Fig. 3a (black-and-white print). In the photograph, the solid internal ring is due to radiation from the RSC, and the outer reference ring is produced by the lens. The theoretical distribution of the radiation of the waves  $F_+(\varphi)$  and  $F_-(\varphi)$  [1] for the case when the protons move along the small bisector, calculated from the formulas of Muzikar [2] and Obrdzalek [9], are given in Fig. 3b.

Calculations show that the sum of the distributions  $F_+(\varphi)$  and  $F_-(\varphi)$  exhibits a practically uniform dependence on the angle  $\varphi$ . Thus, for  $\lambda = 6407 \text{ Å}$  we have  $F_+ + F_- = 0.049479$  at  $\varphi = 0$ , and  $F_+ + F_- = 0.049772$  at  $\varphi = 90^\circ$ , i.e., the non-uniformity of  $F_+ + F_-$  relative to  $\varphi$  does not exceed 0.6%.

When Cerenkov radiation produced by the passage of protons along the  $X_3$  axis is transmitted through a polaroid oriented along the  $X_2$  axis, the  $F_+$  waves should be fully transmitted at  $90^\circ$  (disregarding absorption), and the  $F_-$  waves should vanish at  $\varphi = 0^\circ$ . The result of such an experiment with a polaroid is shown in Fig. 4a, from which it is seen that the emission of  $F^e(\varphi)$  waves is uniform with respect to  $\varphi$  from the  $X_2$  axis almost all the way to the  $X_1$  axis. On the other hand, near the  $X_1$  axis, the  $F^e(\varphi)$  waves vanish abruptly.

The experimental  $F(\varphi)$  dependence obtained by photometry of the color negatives is shown in Fig. 4b. The same figure shows the calculated plots of the intensities of the  $F_+(\varphi)$  and  $F_-(\varphi)$  radiation passing through a polaroid, i.e., plots of  $F_+(\varphi) \cos^2 \alpha$ ,  $F_-(\varphi) \cos^2 \alpha$ , and  $(F_+ + F_-) \cos^2 \alpha$ , where  $\alpha = \tan^{-1}[E_1(\varphi)/E_2(\varphi)]$ , and  $E_1$  and  $E_2$  are the components of the electric vectors along the axis  $X_1$  and  $X_2$ . We see that the experimental and calculated plots of  $F(\varphi)$  are in good agreement in a wide range of  $\varphi$ .

The experimental plot of  $F^e(\varphi)$  at  $\varphi = 0^\circ$ , however, does not decrease to zero, as called for by the calculations (see Fig. 4b), and amounts to about (15–25)% of  $F(\varphi)$  at  $\varphi = 90^\circ$ .

The photometric distribution of the  $F(\varphi)$  waves (passing through a polaroid oriented along the  $X_2$  axis) near the  $X_1$  axis is shown in Fig. 5a, from which it is seen that the abrupt change of  $F(\varphi)$  at  $\varphi \sim 0$  occurs in the interval  $\Delta\varphi = \pm 1.6^\circ$ . Photometry of the section of the

“gap” along the  $X_1$  axis (along the “gap”) yielded the curve shown in Fig. 5b, in the form of a peak with total width  $\Delta\theta = 0.5^\circ$  at half-height. (The photometric curves measured along the “gaps”, on both sides of the radiation-ring diameter at  $\varphi = 0^\circ$  and  $\varphi = 180^\circ$ , are similar in shape but are different, possibly because the protons did not pass through the crystal exactly along the  $X_3$  axis.)

When the polaroid was rotated  $90^\circ$  (the radiation with the electric field along the  $X_1$  axis was transmitted), the result shown in Fig. 6a was obtained. The outer “arcs” are the Cerenkov radiation from the lens, and the inner ones are the radiation from the Rochelle-salt crystal. The intensities of these waves have, besides a smooth variation of  $F(\varphi)$  near the  $X_1$  axis (within the interval  $\Delta\varphi \cong \pm 1.5^\circ$ , a peculiar singularity that is manifest in the photograph by two light points of  $\sim 1$  mm diameter, located along the  $X_1$  axis at  $\varphi = 0$  and  $\varphi = 180^\circ$ . Figure 6b shows the calculated distributions of the waves  $F_+(\varphi) \cos^2 \beta$ ,  $F_-(\varphi) \cos^2 \beta$  and  $(F_+(\varphi) + F_-(\varphi)) \cos^2 \beta$  (where  $\tan \beta = E_2/E_1$ ) and the experimental points obtained by photometry of the negative image. The experimental points were reconciled to the calculated plot at the point  $\varphi = 10^\circ$ . In the wide range of angles  $\varphi$  from  $90^\circ$  to  $10^\circ$ , there is satisfactory agreement between the calculated and experimental data. However, no such appreciable increase of the intensity of the waves

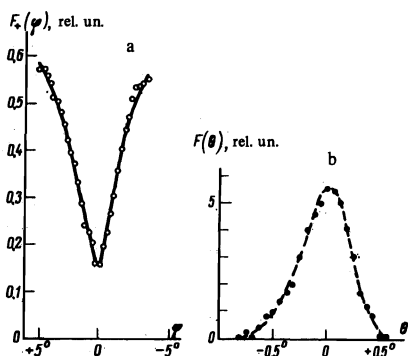


FIG. 5. Photometric curves of  $F(\varphi)$  and  $F(\theta)$ . a— $F_+(\varphi)$  near  $\varphi = 0^\circ$ , b— $F(\theta)$  measured along the “gap”.

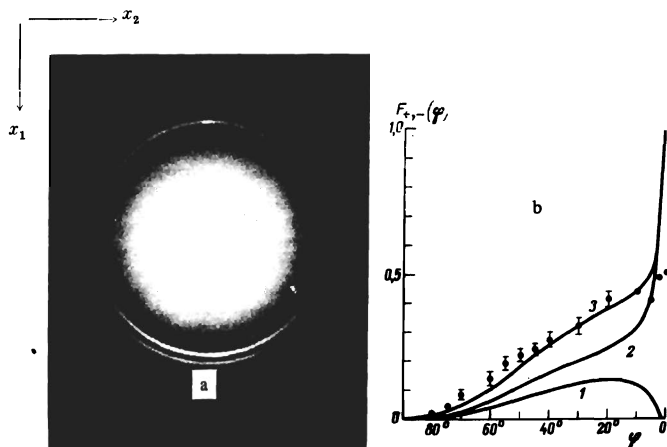


FIG. 6. Intensities of the waves  $F_+(\varphi)$  and  $F_-(\varphi)$  (produced by passage of protons with  $\beta = 0.81$  along the RSC axis), transmitted through a polaroid oriented along the  $X_1$  axis. a—Positive black-and-white images of the radiation obtained in experiment 1. b—Calculated plots: 1— $F_+(\varphi) \cos^2 \beta$ ; 2— $F_-(\varphi) \cos^2 \beta$ , 3— $(F_+(\varphi) + F_-(\varphi)) \cos^2 \beta$  and the experimental points.

$(F_+(\varphi) + F_-(\varphi)) \cos^2 \beta$  is observed near  $\varphi = 0^\circ$ . The apparent reason is that a real particle beam has a spread both in angle and in energy, leading to a smearing of the sharp radiation peak predicted by the theory.

The emission angles  $\theta_+$  and  $\theta_-$  of the extraordinary rays were determined by measuring the diameters of the rings (or “arcs”) of the radiation registered on negative color film (for  $\lambda = 6500 \text{ \AA}$ ) in the direction of the axis  $X_2$  and  $X_1$ . The reference was the radiation ring from a lens (the calculation procedure is described in detail in [2]). The experimental angles  $\theta_{+,-}$  in conjunction with the calculated ones for  $\lambda = 6497 \text{ \AA}$  and  $\beta = 0.81$  are given in Table II. The angles  $\theta_{+,-}^c$  and  $\theta_{+,-}^e$  are in satisfactory agreement within the limits of the angle-measurement errors,  $\Delta\theta = \pm 10'$ .

The aggregate of the experiments on the polarization of the Cerenkov radiation waves due to protons moving along the  $X_3$  axis (along the minor bisector) of RSC show that near the  $X_1$  axis there is a region of radiation with predominant polarization along the  $X_1$  axis, localized in a cone subtending  $\Delta\varphi \approx \pm 1.6^\circ$ .

Thus, it is found that waves with such a polarization are emitted in the form of two narrow beams of light (at angles  $\theta$  to the direction of the particle velocity  $\mathbf{v}$ ) in the plane of the optical axis. We call this “needle radiation” (in analogy with the term Nadelstrahlung used by Einstein [10]).

**Experiment 2.** In this experiment we used an  $X_2$ -cut RSC plate (the particles moved along the  $X_2$  axis). The result of the experiment when the polaroid is oriented along  $X_3$  is shown in Fig. 7a. The same figure shows the calculated distribution of the waves  $F_+(\varphi)$  and  $F_-(\varphi)$  (Fig. 7b). The experimental and calculated distributions are in qualitative agreement. Thus, the waves  $F_+(\varphi)$  have a maximum at  $\varphi = 0$  (reckoned from the  $X_3$  axis), and  $F_-(\varphi)$  have a maximum at  $\varphi = 90^\circ$ , i.e., along  $X_1$ .

The photograph of Fig. 7a shows three sets of arcs. The outer arcs constitute radiation from two plates with  $n_D = 1.564$ , between which the  $X_2$ -cut RSC was placed for the experiments with the electric field (see below). The calculated and experimental radiation angles produced in this case agree with each other and are listed in Table III.

**Experiment 3.** Since the RSC had a polydomain structure, it was natural to investigate the properties of the Cerenkov radiation under conditions in which the domains vanished, i.e., at a temperature  $t > 24^\circ\text{C}$  (above the Curie point), and with an electric field of intensity  $V > 500 \text{ V/cm}$  applied to the crystal, when the RSC changes from polydomain to single-domain.

TABLE II

$\varphi$	Calculated angles for $\lambda = 6497 \text{ \AA}$		Experimental angles	
	$\theta_+^c$	$\theta_-^c$	$\theta_+^e$	$\theta_-^e$
$0^\circ$ (along the $X_1$ axis)	$34^\circ 12.4'$	$33^\circ 58.2'$	—	$33^\circ 57.7'$
$90^\circ$ (along the $X_2$ axis)	$34^\circ 6.7'$	$34^\circ 0.2'$	$33^\circ 59.3'$	—

TABLE III

$\varphi$	Calculated angles		Experimental angles	
	$\theta_+^c$	$\theta_-^c$	$\theta_+^e$	$\theta_-^e$
$0^\circ$ (along the $X_2$ axis)	$34^\circ 8.5'$	$33^\circ 54.1'$	$34^\circ 1.5' \pm 10'$	—
$90^\circ$ (along the $X_1$ axis)	$34^\circ 12.4'$	$33^\circ 55.8'$	—	$33^\circ 48.7' \pm 10'$

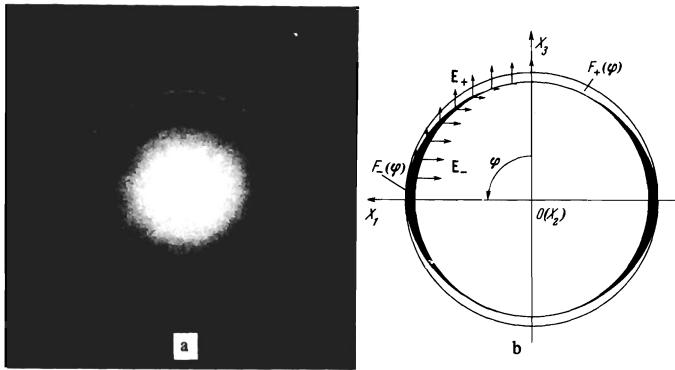


FIG. 7. Experimental and calculated plots of the waves  $F_+(\varphi)$  and  $F_-(\varphi)$  of the Cerenkov radiation produced when protons with  $\beta = 0.81$  move along the  $X_2$  axis ( $X_2$ -cut plate) of RSC. a—Photograph of radiation transmitted through a polaroid oriented along the  $X_3$  axis (inner arcs—RSC radiation, middle arcs—lens radiation, outer arcs—radiation from plates with  $n_D = 1.564$ ). b—Calculated distributions of the waves  $F_+(\varphi)$  and  $F_-(\varphi)$ .

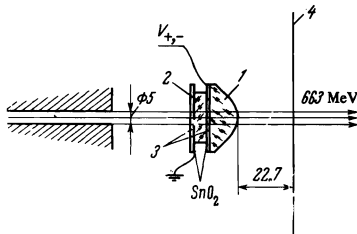


FIG. 8. Experimental setup: 1—plane-parabolic lens with  $f = (22.7 \pm 0.1)$  mm; 2—RSC plate; 3—plates of glass with  $n_D = 1.564$ ; 4—photographic film.

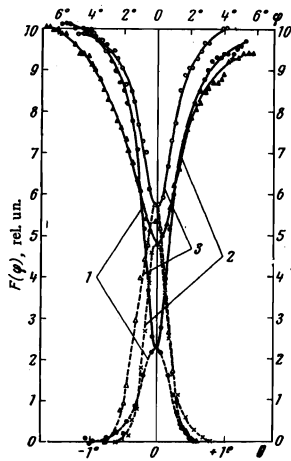


FIG. 9. Photometric distribution curves of the radiation produced by passage of 660 MeV protons along the  $X_3$  axis of RSC and transmitted through a polaroid oriented along the  $X_2$  axis. 1— $F(\varphi)$  and  $F(\theta)$  at  $V = 0$  and  $t < 24^\circ\text{C}$ . 2— $F(\varphi)$  and  $F(\theta)$  at  $V = -1000$  V (voltage applied along the  $X_3$  axis, i.e., along the proton beam). 3— $F(\varphi)$  and  $F(\theta)$  at  $V = 0$  and  $t = 32.3^\circ\text{C}$  ( $t > 24^\circ\text{C}$ ) ( $F(\theta)$ —upper curves,  $F(\theta)$ —lower curves).

The experiment with the electric field applied along the axis  $X_2$  and  $X_3$  and with motion of the protons along the same axis was performed with the setup illustrated in Fig. 8. The  $X_3$ -cut (or  $X_2$ -cut) RSC was placed between two plane-parallel plates of glass with  $n_D = 1.564 \pm 0.001$  of thickness 1 mm, coated with a thin semi-transparent  $\text{SnO}_2$  layer. One  $\text{SnO}_2$  electrode was grounded, and to the other we applied an electric field  $V_+$  or  $V_-$  of intensity up to 2 kV/cm. The optical contact between the RSC and the  $\text{SnO}_2$  layers, as well as between the glass plate and the plane-parabolic lens, was by means of a silicone lubricant. The effect of temperature (at  $t = 32.3^\circ\text{C}$ ) on the properties of the radiation was investigated only for the  $X_3$ -cut plate.

As to the results of these experiments, we can state the following. We observed no changes in the emission angles  $\theta_+$  and  $\theta_-$  for the waves  $F_+$  and  $F_-$  respectively

within the limits of the angle measurement error ( $\Delta\theta = \pm 10'$ ). However, the intensity distribution of the radiation produced by passage of protons along the  $X_3$  axis through a  $X$ -cut plate, near the  $X_1$  axis (along the "gaps") was altered both by the action of the electric field and by the action of the temperature.

Figure 9 shows the experimental distributions  $F(\varphi)$  and  $F(\theta)$  near and along the  $X_1$  axis, respectively, obtained by photometry of the color negatives. The distributions  $F(\varphi)$  were obtained by photometry of the image along a tangent drawn at point  $\varphi = 0$  (perpendicular to the  $X_1$  axis). The distributions  $F(\theta)$  are the results of photometry along the gap (along the  $X_1$  axis).

As seen from the figure, the action of the electric field and of the temperature on  $F(\varphi)$  and  $F(\theta)$  is approximately the same. Both factors fill up the "gap" with radiation polarized perpendicular to the  $X_1$  axis. Thus, whereas the fraction of this radiation at  $V = 0$  was about 25% at the minimum of  $F(\varphi)$ , it increased to (50–60)% at  $V = 1000$  V.

The emission angle corresponding to this peak is  $\theta_x = 34^\circ 3.5' \pm 10'$ , and its total width at half-height is  $\Delta\theta_x = 0.5^\circ$ .

#### 4. SUMMARY OF RESULTS AND DISCUSSION

All the fundamental properties of Cerenkov radiation, predicted by the theory for the biaxial RSC, were confirmed experimentally. We observed no influence of the polydomain structure of the RSC on such radiation properties as directivity, polarization, and azimuthal distribution of the radiation. We revealed a certain discrepancy between the experiment and the theoretical predictions for Cerenkov radiation produced by passage of protons with  $\beta = 0.81$  along the  $X_3$  axis.

One of the possible causes of the appearance of Cerenkov radiation along the  $X_1$  axis may be the angular divergence of the protons in the 660-MeV beam and their scattering in the crystal, which leads to a filling of the "gap" by radiation of  $F_+$  waves, which is quite intense near the  $X_1$  axis (see Fig. 4). Another possible cause of this singularity may be such optical phenomena in biaxial crystals as internal and internal conical refraction.

It is known from crystal optics that internal conical refraction takes place if the waveguide vector of the light wave coincides with the binormal, and external conical refraction takes place when the ray vector coincides with the biradial. For a particle moving along the  $X_3$  axis (minor bisector) of RSC, the condition under which the normal of the Cerenkov radiation wave front coincide with the binormal (condition for internal conical refraction) is<sup>[11]</sup>

$$x^2 = \epsilon_1 \frac{\epsilon_3 - \epsilon_2}{\epsilon_3 - \epsilon_1}, \quad (1)$$

where  $x = 1/\beta$  ( $\beta$  is the particle velocity), and  $\epsilon_1$ ,  $\epsilon_2$  and  $\epsilon_3$  are the principal dielectric constants of the biaxial crystal. At  $\beta = 0.81$ , condition (1) is satisfied in RSC within 2.7% for the long-wave part of the emission spectrum ( $\lambda \sim 6500 \text{ \AA}$ ).

The cone of the internal conical refraction (the ray-vector cone) inside the crystal and in the plane  $X_1OX_3$  is bounded by the biradial

$$\text{tg } \beta = \sqrt{\frac{\epsilon_3(\epsilon_3 - \epsilon_1)}{\epsilon_1(\epsilon_3 - \epsilon_2)}}$$

and by the angle  $\beta_1$ , defined in accordance with<sup>[11]</sup> by the formula

$$\operatorname{tg} \beta_1 = \sqrt{\frac{\epsilon_1(\epsilon_2 - \epsilon_1)}{\epsilon_3(\epsilon_3 - \epsilon_2)}} \quad (2)$$

The cone of the external conical refraction (the wave-vector cone) in the  $X_1OX_2$  plane is bounded by the angles  $\gamma$  and  $\gamma_1$ <sup>[12]</sup>:

$$\gamma = \operatorname{arctg} \left( \sqrt{\frac{\epsilon_1}{\epsilon_3}} \operatorname{tg} \beta \right), \quad \gamma_1 = \operatorname{arctg} \left( \frac{\epsilon_2}{\epsilon_1} \sqrt{\frac{\epsilon_2 - \epsilon_1}{\epsilon_3 - \epsilon_2}} \right) \quad (3)$$

The angles  $\gamma$  and  $\gamma_1$  are measured from the  $X_3$  axis.

Table IV gives the values of the angles  $\theta_-, \beta, \beta_1, \gamma$  and  $\gamma_1$ , calculated in accordance with the corresponding formulas for the values of the RSC at three wavelengths. It is seen from the table that the angles  $\beta, \beta_1, \gamma$ , and  $\gamma_1$  as functions of  $\lambda$  range approximately from 35 to 31°, whereas  $\theta_-(\lambda)$  varies (in the same band  $\Delta\lambda$ ) from 34 to ~35°. Thus, there is a region of  $\Delta\lambda$  where the angles  $\theta_-$  coincide with  $\beta$  and  $\gamma$ .

TABLE IV

Angles	$\lambda = 6497 \text{ \AA}$	$\lambda = 5893 \text{ \AA}$	$\lambda = 4554.2 \text{ \AA}$
$\theta_-(\varphi = 0)$	34°0'10"	34°9'10"	34°39'50"
$\beta$	35°6'38"	35°35'50"	30°47'20"
$\beta_1$	34°54'59"	35°24'20"	30°36'1"
$\gamma$	35°0'48"	35°30'0"	30°41'20"
$\gamma_1$	35°12'28"	35°42'0"	30°53'22"

Outside the RSC, the Cerenkov radiation, after experiencing internal conical refraction, is distributed on the surface of a circular cylinder with a diameter determined by the angle difference  $\Delta\beta = \beta - \beta_1$  (in our case  $\Delta\beta = 11.7'$ ) and by the crystal thickness. At the points where the radiation cones intersect the  $X_1$  axis, the Cerenkov radiation should in principle emerge from two points in the form of additional cones with vertex angles determined by the difference  $\Delta\gamma = \gamma_1 - \gamma$ , owing to the external conical refraction outside the crystal (with allowance for the regular refraction). However, the density of the Cerenkov radiation that experiences both internal and external conical refraction will be insignificant, owing to the distribution of a small part of the main cone of radiation over the cylindrical and conical surfaces of the corresponding refractions.

The following assumption can be advanced concerning the influence of the RSC polydomain structure, observed in experiments with an electric field and with a heated  $X_3$ -cut crystal, on the properties of the radiation (emitted when protons with  $\beta = 0.81$  move along the minor bisector, the  $X_3$  axis) filling the "gaps" and polarized perpendicular to the  $X_1$  axis (and not predicted by the theory). It is known<sup>[13]</sup>, that when an electric field is

applied along the  $X_3$  axis (minor bisector) of an RSC and the temperature of a crystal with domain structure is varied, the optical indicatrix is rotated through a certain angle  $\alpha$  about the  $X_3$  axis. For example, when the crystal is heated from +10 to +25°C, the optical indicatrix of the RSC rotates through an angle  $\alpha \sim 1^\circ$ . This, naturally, can lead to a change in the properties of the Cerenkov radiation emitted by a particle moving along the minor bisector of the RSC.

This effect can be estimated quantitatively only on the basis of the still undeveloped theory of Cerenkov radiation in biaxial crystals with domain structures.

The authors are most grateful to L. A. Shuvalov of the Crystallography Institute of the USSR Academy of Sciences for the Rochelle-salt crystals, to T. I. Kozlova for much photometric work, and to R. Yanik for help with the work.

<sup>1</sup> $F_+(\varphi)$  and  $F_-(\varphi)$  are the azimuthal distributions of extraordinary waves with mutually perpendicular polarization of the Cerenkov radiation in a biaxial crystal.

<sup>1</sup>V. P. Zrelov, Zh. Eksp. Teor. Fiz. **46**, 447 (1964) [Sov. Phys.-JETP **19**, 300 (1964)].

<sup>2</sup>V. P. Zrelov, P. Pavlovic, and P. Sulek, JINR Preprint R1-4364 (1969).

<sup>3</sup>D. Gföller, Zeit. Physik, **183**, 83, 1965.

<sup>4</sup>I. M. Frank, Usp. Fiz. Nauk **30**, 149 (1946).

<sup>5</sup>S. I. Vavilov, Sobr. sochinenii (Collected Works), Vol. 2, AN SSSR, 1952, p. 218.

<sup>6</sup>I. V. Kurchatov, Segnetoelektrichestvo (Ferroelectricity), Gostekhizdat, 1933.

<sup>7</sup>N. R. Ivanov and V. F. Zotov, Kristallografiya **11**, 924 (1966) [Sov. Phys.-Crystallogr. **11**, 781 (1967)].

<sup>8</sup>Nucl. Sc. Series, Report 39, Committee on Nucl. Sc. Publ. 1133. NAS-NRS, Washington, 1964.

<sup>9</sup>J. Obdržálek, Czech. J. Phys. **B19**, 1556, 1969.

<sup>10</sup>A. Einstein, Collected Works (Russ. transl.), Vol. 3, Nauka, 1966, p. 153 (Comment on P. Jordan's article "On the Theory of Quantum Emission").

<sup>11</sup>V. P. Zrelov, Izluchenie Vavilova-Cherenkova i ego primenenie v fizike vysokikh énergií (Vavilov-Cerenkov Radiation and Its Applications in High Energy Physics), Part 1, Atomizdat, 1968, p. 207.

<sup>12</sup>L. D. Landau and E. M. Lifshitz, Élektrodinamika sploshnykh sred (Electrodynamics of Continuous Media), Gostekhizdat, 1957, p. 413 [Pergamon, 1959].

<sup>13</sup>I. S. Zheludev, Usp. Fiz. Nauk **88**, 253 (1966) [Sov. Phys.-Uspekhi **9**, 97 (1966)].

Translated by J. G. Adashko

26